# Leidenfrost spheres, projectiles, and model boats: Assessing the drag reduction by superhydrophobic surfaces

Ivan U. Vakarelski [a,b,*], Farrukh Kamoliddinov [a], Aditya Jetly [a], Sigurdur T. Thoroddsen [a]

[a] *Division of Physical Sciences and Engineering, King Abdullah University of Science and Technology (KAUST), Thuwal 23955-6900, Saudi Arabia*
[b] *Department of Chemical and Pharmaceutical Engineering, Faculty of Chemistry and Pharmacy, Sofia University, 1 James Bourchier Avenue1 James Bourchier Avenue, Sofia 1164, Bulgaria*

HIGHLIGHTS

- Drag reduction by Leidenfrost vapor layers predict the limit for superhydrophobic surfaces drag reduction.
- For spheres there is a dramatic effect due to early drag crises.
- For streamlined projectile and model boats the drag reduction is moderate.
- For sub-critical Reynolds numbers skin friction is less sensitive than form drag to the gas layer effects.

GRAPHICAL ABSTRACT
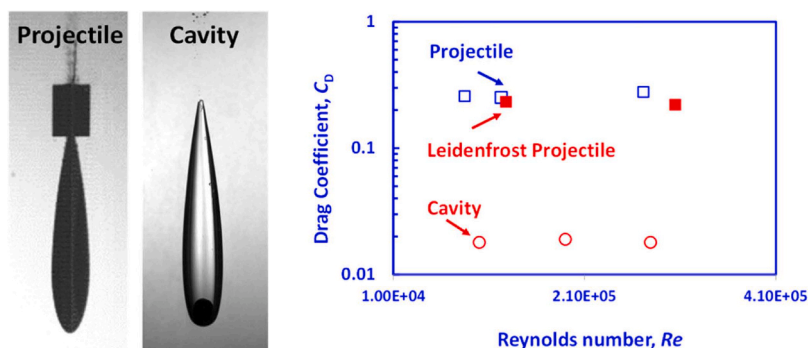
ARTICLE INFO

ABSTRACT

Superhydrophobic surfaces are expected to reduce drag on bluff bodies moving in water due to the introduction of a thin air layer around the solid and the resulting partial slip boundary condition. The use of Leidenfrost vapor layers, sustained on the surface of a heated metal body is a reliable method to estimate the maximum drag reduction possible due to such air layers. In the past such an approach was used to estimate the drag reduction on a free-falling heated sphere, in which case the form drag is the lead component of the drag force. Here, we extend this approach to evaluate the effect of the thin gas layers on the hydrodynamic drag of free-falling streamlined projectiles and towed model boats, where the form drag is minimal, and the skin friction drag is the lead component of the drag force. By comparing the drag for streamlined bodies with and without sustained air-layers, we see only incremental drag reductions, for the sub-critical Reynolds number tested herein. The same is true for towed model boats. These results hold both for superhydrophobic surface treatments and Leidenfrost vapor layers. Thus, we concluded that for the investigated range of sub-critical Reynolds numbers, the skin friction drag is less sensitive to the effect of the thin gas layers compared to the form drag. These novel findings have important implications for the practical potential of energy savings using gas layers sustained on superhydrophobic surfaces.

* Corresponding author at: Division of Physical Sciences and Engineering, King Abdullah University of Science and Technology (KAUST), Thuwal 23955-6900, Saudi Arabia

E-mail address: ivakarelski@lcpe.uni-sofia.bg (I.U. Vakarelski).

1. Introduction

Introducing a gas layer on the surface of a solid body moving in liquid can significantly lower hydrodynamic drag and be used to reduce energy consumption on marine vessels. Some methods to introduce the gas layer at the solid interface include bubble injection, cavitation, supercavitation [1–4] and superhydrophobic surfaces that can naturally sustain a thin air layer underwater, referred to as a plastron [5–12]. The underlying physical mechanism through which the drag is reduced relates to the exchange of the no-slip boundary condition at the solid-liquid interface with a partial slip boundary condition at the liquid - gas layer - solid interface, which can be formally quantified using an effective slip length [13–17]. The use of a superhydrophobic surface is particularly attractive because it is a passive method to sustain the gas layer that does not require additional energy input. However, despite the intense research effort in the last two decades, the practical applications of superhydrophobic surfaces for effective drag reduction have been limited. Some of the reasons for this are the poor mechanical durability of the plastron under shear stress and its tendency to dissolve with time [9–12].

An alternative approach to examine the effect of gas layers on hydrodynamic drag is the use of a Leidenfrost vapor layer sustained on the surfaces of heated solids in contact with liquid [18–24]. Pioneering experiments were done with heated metallic spheres free-falling in a fluorocarbon liquid [20]. The fluorocarbon liquid used in this investigation (FC-72, perfluorohexane) has a low boiling point and low vaporization heat capacity, which makes it easier to sustain a stable vapor layer on the surface of the heated sphere. It was demonstrated that introducing the vapor layer resulted in up to 90 % drag reduction, pronounced as an early drag crisis transition [20,23]. The conventional drag crisis transition is the phenomenon of the sudden drop of the drag coefficient on a smooth sphere, $C_D = 2F_D/(\pi R^2 \rho U^2)$, when the Reynolds number, $Re = 2\rho R U/\mu$ reaches $\sim 3 \times 10^5$ [25]. Here, F_D is the hydrodynamic drag force on the sphere of radius R traveling with velocity U in a fluid of density ρ and dynamic viscosity μ. Later experiments demonstrated similar effects in the case of a heated metallic sphere free-falling in water [21]. However, because of the high vaporization heat capacity of room temperature water, in this case, experiments were conducted near the boiling temperature of water. For a narrower range of Reynolds numbers near the drag crisis, the effect of the early transition was also observed using a thin air layer plastron sustained on the surface of a superhydrophobic sphere free-falling in room temperature water [26, 27]. The narrower range of the drag reduction for the plastron is expected, considering that the Leidenfrost vapor layers were the order of magnitude thicker than the plastrons.

Experiments with free-falling spheres demonstrated that the Leidenfrost vapor layer results could predict the maximum drag reduction that can be expected using plastrons sustained on a superhydrophobic surface. In the present work, we aim to extend this approach to the case of free-falling streamlined projectile and towed model boats. Spheres represent a bluff body, where the primary drag is the pressure-induced form drag. In contrast, for streamlined projectiles and the model boat investigated here, the lead drag contribution is expected to be the liquid-viscosity-related skin friction drag.

A further motivation for the present investigation is the recently discovered phenomenon of sphere encapsulation in a stable streamlined gas cavity following the sphere impact on a liquid held in a deep tank [28–30]. This phenomenon was observed for the impact of heated metallic spheres on perfluorohexane or 95 °C water, as well as for the impact of superhydrophobic spheres on room temperature water [28, 29]. An example is shown in Fig. 1b for the case of a heated steel sphere in perfluorohexane and in Fig. 1d for the case of a heated tungsten carbide sphere in 95 °C water. A similar phenomenon was later demonstrated for the high-velocity impact of a non-superhydrophobic sphere on room temperature water, in which case the streamlined cavity was attached just above the sphere's equator [30]. In all cases,

because of the low viscous friction along the cavity interface, the sphere-in-air-cavity formations were found to have an order of magnitude lower drag coefficients than similar-shape solid projectiles. Here by using alumina projectiles that have a similar shape to that of the sphere-in-air-cavity formations, we evaluate to what extent the drag could be reduced by using a plastron on superhydrophobic projectile or by using sustained Leidenfrost vapor layer on a heated projectile (Fig. 1).

2. Experimental

In our experiments, we use high-speed camera imaging to monitor the free-fall of the streamlined projectiles in a liquid tank or the movement of a model boat towed along the surface of a liquid channel. Most of the experiments follow protocols and characterization processes given in our prior studies with free-falling spheres [20–23,27], model boats [31], and horizontally pulled spheres [32,33]. Below we give the specific details for each of the present experiments.

2.1. Horizontally pulled sphere

Experiments with horizontally pulled alumina spheres were conducted in the KAUST water channel, which is 10 m long and has a 1×1 m cross-section. The channel's walls are made from transparent clear acrylic, allowing side-view observations. The primary experiments conducted in the channel were for a model boat or floating hollow aluminum sphere towed along the water-air interface using a counter-weight pulley system [31–33]. In the present work, we use the same set-up to pull a neutrally buoyant hollow alumina sphere under water. The sphere has an outer diameter of 10 cm, and the sphere wall thickness was adjusted to achieve a neutral buoyancy, e. g. the effective sphere density equals the density of water. Further details on the horizontally pulled sphere experiments can be found in our recent related studies [32,33].

2.2. Free-falling projectiles

Two alumina streamlined shape projectiles were used. Pictures of the two projectiles are shown in Supplementary Figure S1. As demonstrated in Fig. 1, the projectiles' shape and dimensions were chosen to approximately match the Leidenfrost sphere with streamlined cavity formations that were investigated in our prior studies. The shorter projectile has a length, $L = 7.0$ cm, diameter, $D = 2.33$ cm, and weight of 82 g (Figure S1a and Fig. 1a). The longer projectile has a length, $L = 12.5$ cm diameter, $D = 2.5$ cm, and weight of 115 g (Figure S1b and
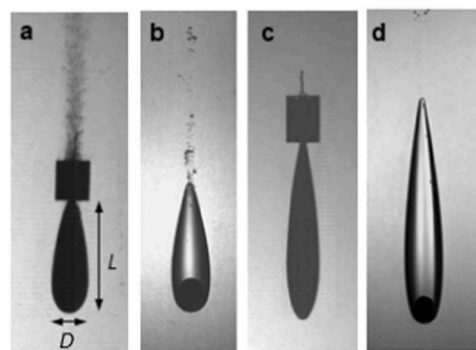

Fig. 1. High-speed camera snapshots of free-falling alumina projectiles and similar shaped spheres-with-air-cavity formations. (a) Heated $L/D = 3.0$ projectile falling in FC-72, (b) $L/D = 3.0$, 20-mm-diameter heated steel sphere with cavity formation falling in perfluorohexane. (c) Heated $L/D = 5.0$ projectile falling in 95 °C water, (d) $L/D = 5.0$, 20-mm-diameter heated tungsten carbide sphere with cavity falling in 95 °C water. Images (b) and (d) are adopted from Vakarelski et al. 2017 [29].

Fig. 1c). For brevity, we will refer to them as the short ($L/D = 3$) and the long ($L/D = 5$) projectile. Tail stabilizers at the back of the projectiles are to maintain a rectilinear trajectory and have been estimated to contribute less than 10 % of the total drag on the projectiles [29].

The drag on free-falling projectiles experiments were conducted in a liquid tank that is 2 m tall and has a square cross-sectional area of 20 × 20 cm, with front and back walls of double-glazed glass windows. An electric heater was installed at the bottom of this tank that allowed the water to be heated up to the boiling point of about 100 °C [21,27].

2.3. Towed model boat

A picture of the alumina model boat used in our experiment is shown in Supplementary Figure S2a, and the boat dimensions in Figure S2b. The boat has a total length of 14 cm, a width of 4 cm, and a wall height of 8 cm. The thickness of the boat bottom of 5 mm and side walls of 3 mm were chosen to allow the boat to float on both water and FC-72. When towed, a plastic vertical fin was mounted on the backs of the boat to maintain a straight trajectory.

The experiments with the model boat were conducted in a liquid channel made of a clear acrylic, of a length of 1.80 m, 30 cm width, and 30 cm height. In the present experiment, the channel was half-filled with water or FC-72 to about 15 cm depth. A pulley system was used to tow the boat in the tank using counterweights as schematized in Supplementary Figure S2c. A fine fishing line (0.2 mm) is hooked to the front of the boat and passed through the pulley system. At the end of the line, we fixed a counterweight whose mass could be adjusted to vary the pulling force.

2.4. Superhydrophobic coating

As in our prior work on metallic spheres, the surfaces of the alumina projectiles, alumina sphere and the model alumina boat were made superhydrophobic by the application of a commercial glass coating: Glaco Mirror Coat Zero (Soft 99 Ltd., Japan). The Glaco is an alcohol-based dispersion of silica nanoparticles ($\sim$ 40 nm) coated with a silane hydrophobic agent. Details on the coating process and surface characterization can be found in our prior work [27,31,34]. In brief, the surfaces were washed with the Glaco and dried at a temperature of about 160 ºC to help consolidate the coating. The coating process is repeated 2–4 times, resulting in excellent water repellence of the surfaces. Fig. 2a is a picture of the superhydrophobic long projectile immersed in water, showing the silver mirror shine appearance due to the reflection from the thin air layer plastron. The thickness of the plastron for this coating was estimated to be a few microns (1.0 – 3.0 µm) [27].

After washing with acetone, ethanol and water, the clean alumina sphere, alumina projectile or model alumina boat surface is hydrophilic with an apparent water contact angle of less than 30° [32]. After heating to 280° C and following the experiments in FC-72 or water, the alumina surface remains hydrophilic with apparent water contact angle of less than 45°. Following coating with Glaco the alumina surfaces are superhydrophobic with an advance contact angle of 170° ± 5° and receding contact angle of 160° ± 5° [34]. After experimental runs in water, the Glaco-coated surfaces were confirmed to remain superhydrophobic with the same contact angles characteristics.

2.5. Leidenfrost regime

In all experiments with heated alumina projectiles and model boats, they were kept for at least 30 minutes in a regulated temperature furnace set at 280 ºC before conducting the experiment.

The fluorocarbon fluid used (FC-72, 3 M™ Fluorinert™ Electronic Liquids) is mainly composed of perfluorohexane (C_6F_{14}). It has a boiling point of about 57 ºC, the heat of vaporization, $H_C = 88$ kJ/kg, liquid density $\rho = 1680$ kg/m³, and the dynamic viscosity at room temperature of about 21 ºC was measured to be $\mu = 0.74 \pm 0.01$ mPa s. The low
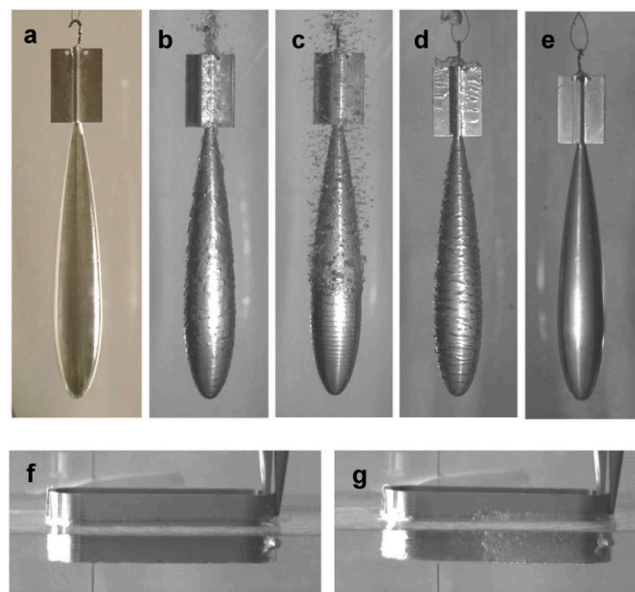

Fig. 2. (a) Picture of the long superhydrophobic projectile dipped in room temperature water showing the silver-mirror sheen appearance of the air plastron. (b, c) High-speed camera snapshots showing the cooling of the long alumina projectile held in FC-72 when initially heated to 280 °C, (b) during the Leidenfrost regime, and (c) during the break-up of the Leidenfrost vapor layer into rising bubbles. (d, e) The cooling of the superhydrophobic projectile in 95 °C water when initially heated to 280 °C, (d) during the Leidenfrost regime, and (e) when the projectile cools to the pool temperature. (f, g) The cooling of the model alumina boat held at the free surface of FC-72, when initially heated to 280 °C, (f) during the Leidenfrost regime, and (g) during the break-up of the Leidenfrost vapor layer.

boiling point and heat of vaporization of FC-72 make it easier to sustain the stable vapor layer in the Leidenfrost regime.

As previously done for the spheres, [20,34] here we used high-speed camera imaging to characterize the cooling of the projectiles and model boats in the FC-72 liquid. Fig. 2b shows a snapshot of the long projectile held in FC-72 when the projectile temperature is above the Leidenfrost temperature $T_L \sim 110$ ºC, and Fig. 2c shows the projectile during the break-up of the Leidenfrost vapor layer. It took about 30 seconds for the projectile that was initially heated to 280 °C to cool to the Leidenfrost temperature in FC-72. As the duration of our experiments is only a few seconds, this guarantees that the projectiles heated to 280 °C before release in the tank, falls in the Leidenfrost regime. A similar characterization was done for the model alumina boat. It took about 25 seconds for the alumina boat held stationary in FC-72 to cool from 280 ºC to $T_L \sim$ 110 ºC (Fig. 2f and Fig. 2g).

As it is difficult to maintain a stable Leidenfrost layer on a sphere or projectile free-falling in room-temperature water, an alternative approach is to conduct experiments in water heated to near the boiling point [21]. The 95 °C water used in our experiments has a density $\rho = 961$ kg/m³ and dynamic viscosity $\mu = 0.30 \pm 0.01$ mPa s. The stability of the Leidenfrost state on the free-falling projectiles was further improved by using superhydrophobic projectiles, which practically remove the nucleate boiling phase during the cooling of the heated projectile statically held in water [21,34]. Fig. 2d shows a high-speed camera snapshot of the superhydrophobic long projectile cooling in 95 °C water during the Leidenfrost regime, and Fig. 2e when cooled to the pool temperature. For a projectile heated to 280 °C, it takes about 50 seconds to cool to the pool temperature of 95 °C. This secures that the 280 °C heated superhydrophobic projectile is in the Leidenfrost regime during the entire fall in the 95 °C water tank.

Whereas the cooling rate on a free-falling projectile or towed model boat could be higher than that on a stationary one, it was always visually

confirmed that the Leidenfrost regime was sustained on the free-falling projectiles and towed model boats during the experimental runs, which lasted only a few seconds. For the conditions of our experiments, the Leidenfrost vapor layer thickness is estimated to be in the range of 100–200 μm in FC-72 [20] and about 100 μm in 95 °C water [21] and thus always significantly thicker than the plastrons sustained on superhydrophobic surfaces.

2.6. Drag coefficient determination

In all experiments, high-speed imaging was performed with a Photron FASTCAM SA5 high-speed video camera. We use a typical filming rate of 2000 frames per second (fps) in the case of the free-falling projectiles and horizontally pulled spheres or 250 fps in the experiments of the towed model boats. All supplemental videos are played back at 30 fps. The velocity of the projectiles, spheres, or model boats was evaluated from the high-speed videos using the camera software (Photron FASTCAM Viewer 4). In all cases, it was confirmed that the projectile, sphere, or model boat had reached the terminal velocity for the respective experiment (Supplementary Figure S3a for projectiles and Figure S3b for boats).

As usual, the drag is evaluated as a dependence of the drag coefficient, C_D, on the Reynolds number, Re. In the case of a sphere moving with steady velocity U,

$$Re = 2\rho R U/\mu \qquad (1)$$

$$C_D = 2F_D/(\pi R^2 \rho U^2) \qquad (2)$$

For a free-falling sphere moving at terminal velocity U, $F_D = (4\pi/3)g$ $[\rho_S - \rho]R^3$, where ρ_S is the sphere density. In the case of the horizontally pulled neutrally-buoyant sphere moving at steady velocity U, $F_D = F_{pull}$, where F_{pull} is the pulling force that is adjusted by varying the counterweight.

In the case of the projectiles, we use the same definitions for the Reynolds number, Re, given by Eq. (1) and drag coefficient, C_D, given by Eq. (2), but this time $R = D/2$, where D is the projectile maximum transverse diameter (Fig. 1a). Correspondingly, for a projectile falling at terminal velocity U, $F_D = g[m_P - \rho V_P]$, where m_P is the projectile mass, and V_P is the projectile volume.

3. Results and discussions

3.1. Drag on spheres

First, we briefly review the effect of the superhydrophobic surfaces plastron and the Leidenfrost vapor layer on the drag of free-falling spheres. Fig. 3 compares selected experimental results from our prior studies for the drag on steel spheres in FC-72, 95 °C water, and room temperature, 21 °C water. For the case of FC-72 and 95 °C water, we compare the fall of the unheated sphere with the heated sphere falling in the Leidenfrost regime. We also compare the unmodified spheres with the superhydrophobic-surface spheres falling in room temperature water. The experiments were conducted for spheres of Reynold numbers between 10^4 and 10^6, covering the drag crisis transition.

For a smooth no-gas-layer sphere, the drag crisis transition to lower drag occurs at Re ~3×10^5. As shown in Fig. 3, for the gas layer-covered sphere, the transition from the subcritical drag coefficient values of 0.45–0.55 to the much lower values of less than 0.1 occurs at lower Re compared to the no-gas-layer spheres. At this, the transition for the Leidenfrost spheres in FC-72 and 95 °C water starts at a lower Re than for the superhydrophobic spheres (see the arrows in Fig. 3). The earlier transition to lower drag for the Leidenfrost vapor layer compared to the superhydrophobic plastron spheres is expected, considering that the Leidenfrost vapor layer is much thicker than the plastron (50–150 μm vs. 1–3 μm) and is fully detached from the solid interface. The free-falling sphere results demonstrate that the Leidenfrost vapor layer drag
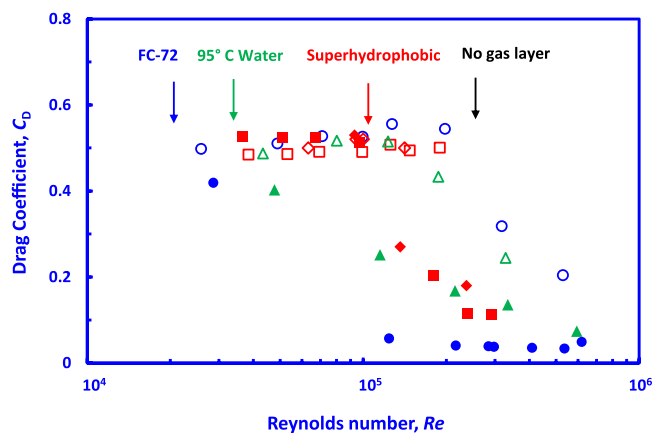

Fig. 3. Variation of the drag coefficient, C_D, with the Reynolds number, Re, for free-falling spheres. Data for the sphere in FC-72 without a vapor layer (open blue circles) and in the Leidenfrost regime (solid blue circles) are taken from Jetly et al. 2019 [23]; data for the sphere in 95 °C water without a vapor layer (empty green triangles) and in Leidenfrost regime (solid green triangles) are from Vakarelski et al. 2016 [21]; data for room temperature water unmodified (empty red squares) and superhydrophobic (solid red squares) spheres are from Jetly et al. 2018 [27]. The figure also shows data for the unmodified (empty red diamonds) and superhydrophobic (solid red diamonds) neutral buoyancy spheres horizontally pulled in room temperature water. Arrows indicate the approximate beginning of the drag crisis transition in each case.

reduction can be used to predict the upper limit of the drag reduction due to any plastron on superhydrophobic surface.

In addition to the free-falling sphere experiments, we have recently conducted experiments on buoyant spheres pulled horizontally in a water channel [32,33]. Using the same water-channel setup, we compare the drag on a neutral buoyancy (with sphere density equal to the water density) unmodified and superhydrophobic spheres pulled horizontally underwater. Supplementary material Video 1 shows an example of such an experiment, showing in parallel the movement of the unmodified and superhydrophobic surface, hollow alumina spheres (10 cm in diameter) pulled with a horizontal force of 7.2 N. The steady velocity of an unmodified sphere is about 1.4 m/s giving $C_D = 0.50$ at $Re = 1.4 \times 10^5$, while for the superhydrophobic sphere, U=2.3 m/s giving $C_D = 0.18$ at $Re = 2.4 \times 10^5$. Data for C_D vs. Re for several pulling forces shown in Fig. 3 agree with the results of Jetly et al. [27] for free-falling spheres. These experiments confirm the capacity of the plastron to reduce drag on bluff bodies in the vicinity of the drag crisis transition. One important observation in the horizontally pulled spheres experiments was that small bubbles were seen to be shed from plastron (Video 1). Because a thicker plastron will be even more susceptible to shear, the use of a thicker plastron might not improve the drag reduction at high shear rates.

Supplementary material related to this article can be found online at doi:10.1016/j.colsurfa.2024.134573.

The drag on bodies moving in bulk liquid is composed of two major components: the pressure-induced form or wake drag, and the viscous or skin friction drag. For spheres falling at sub-critical Reynold numbers, the leading contribution to the drag is the form drag, with the skin friction drag causing less than 5 % of the total drag on the sphere [25]. Correspondingly, the gas layer drag-reduction effects in the vicinity of the drag crisis are due to the lowering of the form drag by moving the flow separation point toward the back of the spheres [20,21,27]. At the same time, for this Reynolds number range, the experiments are not sensitive to the changes in the skin friction drag. With the present experimental study of streamlined projectile and model boat, we extend the Leidenfrost vapor layer approach to estimate the drag reduction to streamlined bodies for which the skin friction is expected to be the dominant drag component.

3.2. Drag on free-falling streamlined projectiles

Next, we compare the drag on free-falling streamlined bodies with and without surface air-layers. We test unmodified and superhydrophobic coating alumina projectiles, at room temperature, 21 °C water, and the drag on projectiles unheated and heated above the Leidenfrost temperature in FC-72 and 95 °C water. A similar experimental protocol was followed as in the case of the free-falling spheres. Fig. 4 summarizes the drag coefficient, C_D vs. Reynolds numbers, Re, values obtained in these experiments, and Supplemental Videos 2, 3, and 4 parallel the fall of the long projectile for the respective no-gas layer and gas-layer cases.

Supplementary material related to this article can be found online at doi:10.1016/j.colsurfa.2024.134573.

Video 2 shows the free-fall of the long ($L/D = 5.0$) projectile in room temperature water, paralleling the fall of the unmodified and superhydrophobic coating projectile. No significant difference was found in the terminal fall velocity and the respective drag between the unmodified and superhydrophobic projectiles. For the short ($L/D = 3.0$) projectiles, as well, no differences in the unmodified and superhydrophobic projectile fall velocity were observed. The terminal velocity for the shorter projectiles was about 3.7 m/s giving $C_D = 0.19$ at $Re = 8.8 \times 10^4$, and for the long projectiles, about 3.4 m/s giving $C_D = 0.25$ at $Re = 8.5 \times 10^4$. The higher drag for the longer projectile indicates the increase in the skin friction along the length of the projectiles, confirming that skin friction becomes the dominant drag component for the streamlined projectiles. Thereby, we conclude that the lack of drag reduction in these experiments indicates that for the sub-critical Reynolds number range investigated here, the skin friction might not be as sensitive to the plastron as it is for the form drag on the spheres in the vicinity of the drag crisis transition.

Next, we investigate the gas layer effects in the case of a Leidenfrost vapor layer. Video 3 shows the fall of the long projectile in FC-72 liquid, paralleling the fall of the unheated projectile and the 280 °C heated projectile falling in the Leidenfrost regime. As seen in the video, the fall velocity of the Leidenfrost projectiles is only marginally higher than that of the unheated projectile. Similar results were obtained for the short projectile. Because the projectiles experiment in room temperature water and in FC-72 are at similar Reynolds numbers the lack of effect by the superhydrophobic plastron agrees with the marginal effect due to the Leidenfrost vapor layer. This further demonstrates that the skin friction at that Reynolds numbers range is not that sensitive to the

presence of thin gas layers at the interface of the streamlined bodies, even when the thicker Leidenfrost vapor layers are present.

Similarly, to the room temperature water experiments, initial runs in 95 °C water showed no difference in the fall velocity of the unmodified and the superhydrophobic coating projectiles. The same result was observed for projectiles initially heated to the pool temperature of about 95 °C. Following, we compared the fall velocity of the unheated superhydrophobic projectile and the superhydrophobic projectile heated to 280 °C. Video 4 parallels the fall of the long superhydrophobic projectile in 95 °C water for the unheated and the heated to 280 °C projectile falling in the Leidenfrost regime. In this case, the Leidenfrost projectile terminal velocity is moderately increased compared to the no gas layer projectile resulting in a 20 % decrease in the drag coefficient. A similar drag decrease of about 15 % was measured for the shorter projectile (Fig. 4).

The larger drag reduction by the Leidenfrost vapor layer for the 95 °C water compared to the FC-72 could be due to the higher Reynolds number, $Re \approx 3 \times 10^5$ approaching the drag crisis transition. Nevertheless, the observed drag decrease is moderate compared to the one measured for the sphere at the same Reynold numbers range, and the extremely low drag on the similar shaped sphere-with-air-cavity formation which are included in Fig. 4 for comparison [29]. Clearly, the reduction in the skin friction due to the introduction of the thin vapor layer is not comparable to the reduction of the skin friction due to the exchange of the solid-liquid with solid-gas interface in the case of the sphere with cavity formation.

3.3. Drag on a towed model boat

In the following, we measure the drag on the alumina model boat towed in the liquid test channel. In the first set of experiments, the unmodified and the superhydrophobic coating boats were towed in the channel filled with room temperature water. In the second set of experiments, the unheated and heated to 280 °C alumina boat moving in the Leidenfrost regime was towed in the channel filled with FC-72.

Results for the unmodified and superhydrophobic boat's measured velocities vs. towing force are presented in Fig. 5a. Composite Video 5 is an example showing in parallel the movement of the unmodified and superhydrophobic coating boat in the water channel when pulled with a towing force of 0.03 N. As seen in the video and Fig. 5a, there was no measurable difference between the unmodified and the superhydrophobic boats for the entire pulling force range. This result for the drag on the superhydrophobic coating boat agrees with our recent study, where similar measurements were conducted using a 30 cm long high-speed hull model boat [31]. In that study, no differences in the velocities of the unmodified and superhydrophobic coating boats were found when the boats were powered by an electric engine or towed with a pulley system like the one in the present study. However, in the higher speed regime (1–2 m/s), the plastron had a pronounced effect on the splashing patterns around the boat hull [31]. Because of the high speed of the boats in that prior study, apart from the skin and form drag, the wave drag was a major component of the total drag. The shape of the boat hull in the present study and the much lower speeds used suggest that the drag on the model alumina boats here is dominated by the skin friction drag.

Supplementary material related to this article can be found online at doi:10.1016/j.colsurfa.2024.134573.

One reason that our measurements did not find any decrease in the hydrodynamic drag on the superhydrophobic boats, whereas similar studies with model boats by other groups claim a significant effect [35–37], could be the thickness of the superhydrophobic surfaces plastron used in different studies. If this is the case, the Leidenfrost vapor layer experiments are expected to indicate the upper limit of the drag reduction by the thicker air plastrons. Results for the velocity dependence on the pulling forces in the FC-72 filled test channel for the unheated and heated to 280 °C boat that is moving in the Leidenfrost
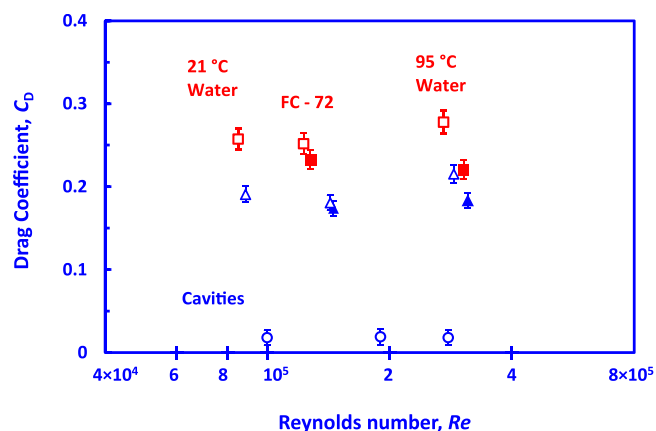

Fig. 4. Variation of the drag coefficient, C_D, with the Reynolds number, Re, for the unheated $L/D = 3.0$ projectile (open blue triangles) and $L/D = 5.0$ projectile (open red squares), and heated projectiles falling in Leidenfrost regime for the $L/D = 3.0$ (solid blue triangles) and $L/D = 5.0$ projectile (solid red squares), falling in 21 °C water, FC-72 and 95 °C water. Data for $L/D = 5.0$ sphere-with-air-cavity formation falling in 95 °C water with much lower C_D is also shown (open blue circles) [29].
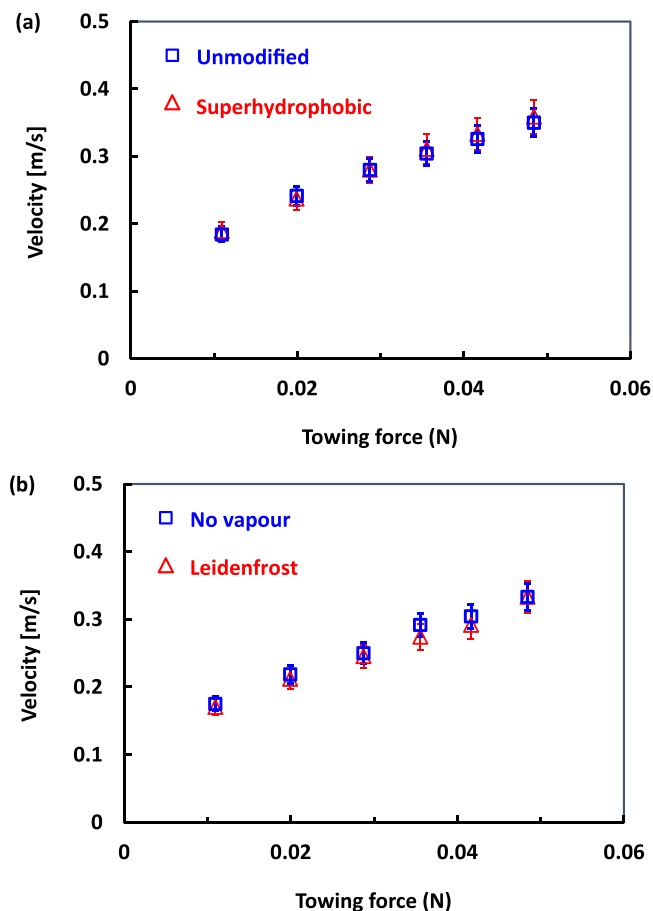
Fig. 5. The velocity of model boats towed along a free liquid surface. (a) The velocity of the alumina model boat vs towing force, for the unmodified boat (empty blue squares) and the superhydrophobic hull boat (empty red triangles) towed in water. (b) Dependence of the alumina model boat velocity on the towing force for the unheated boat (empty blue squares) and heated to 280 °C boat (empty red triangles) moving in Leidenfrost regime towed in the FC-72.

regime are compared in Fig. 5b. Video 6 is an example paralleling the movement of the unheated and Leidenfrost boat when pulled with a towing force of 0.03 N. It is seen that for the entire range of the pulling forces used no significant difference was found in the velocities of the no vapor layer and Leidenfrost vapor layer boats.

Supplementary material related to this article can be found online at doi:10.1016/j.colsurfa.2024.134573.

Considering that even the thick and sustainable Leidenfrost vapor layer did not produce a measurable reduction of the drag on the model boat and on the alumina projectiles away from the drag crisis transition, it is unrealistic to expect a significant drag reduction due to any plastrons sustained on superhydrophobic surfaces. Our experiments confirm that, indeed, and it is unlikely these results will change if a thicker plastron is used by applying alternative superhydrophobic coatings.

The experimental trend found here, that over the studied range of Reynolds numbers the skin friction drag is less sensitive to the introduction of a vapor layer compared with the form drag agrees with a recent numerical study on the effect of the vapor layer on the drag of spheres moving at moderate Reynolds numbers [16]. To capture the vapor layer effect, the study by Berry et al. [16] uses a Navier slip model defined by an effective slip length scaled with the sphere radius, λ_S/R. The model predicts that for $10^2 < Re < 4 \times 10^4$, the delay of the flow separation induced even by small slip lengths that have little effect on the skin friction drag could significantly affect the pressure drags. In a later study Arrieta and Sevilla, proposed a more detailed model including explicitly the role of the vapor layer on a solid sphere [17],

and reached the conclusion that the dominant mechanism responsible for the later separation of the flow is the onset of vapor recirculation caused by the adverse pressure gradient in the rearward half of the sphere. In future investigations similar models could be adopted to quantify the gas layer effect on the drag on streamlined projectiles and model boats.

4. Conclusion

We investigate the effects of Leidenfrost vapor layers on the movement of solid bodies in liquids and how they can be used to predict drag reduction due to thin air-layer plastrons sustained on superhydrophobic surfaces. In the case of a sphere which is a typical bluff body, the Leidenfrost vapor layers dramatically affect the drag by lowering the Reynolds number at which the drag crisis transition occurs, resulting in an order of magnitude decrease in drag coefficient compared to the no-vapour-layers case. This drag-reduction effect is mirrored for free-falling and horizontally pulled superhydrophobic spheres in the vicinity of the drag crisis transition.

In the case of the streamlined projectile for which the skin friction is the main drag component, using Leidenfrost vapor layers has a moderate effect on the total drag force. In agreement with this, there was no measurable effect due to the plastron on the superhydrophobic surfaces, for the drag on free-falling streamlined projectiles. Similarly, there was no effect on the drag due to Leidenfrost vapor layers or super-hydrophobic surface plastron for a model boat for which the skin friction drag is the dominant drag component.

Our study indicates that for the studied range of sub-critical Reynolds numbers, compared to the form drag the skin friction drag is far less sensitive to the introduction of thin gas layers. However, one should remember that different dependencies are expected to hold for higher Reynolds numbers turbulent flow, or lower Reynolds numbers Stokes flow.

CRediT authorship contribution statement

Ivan U. Vakarelski: Writing – original draft, Methodology, Investigation, Conceptualization. **Farrukh Kamoliddinov:** Investigation. **Aditya Jetly:** Investigation. **Sigurdur T. Thoroddsen:** Writing – review & editing, Supervision, Methodology.

Declaration of Competing Interest

The authors declare that they have no known competing financial interests or personal relationships that could have appeared to influence the work reported in this paper.

Data availability

Data will be made available on request.

Appendix A. Supporting information

Supplementary data associated with this article can be found in the online version at doi:10.1016/j.colsurfa.2024.134573.

References

[1] S.L. Ceccio, Friction drag reduction of external flows with bubble and gas injection, Annu. Rev. Fluid Mech. 42 (2010) 183–203.

[2] Y. Murai, Frictional drag reduction by bubble injection, Exp. Fluids 55 (2014) 1773.

[3] H. Wang, K. Wang, G. Liu, Drag reduction by gas lubrication with bubbles, Ocean Eng. 258 (2022) 111833.

[4] D. Yang, Y.L. Xiong, X.F. Guo, Drag reduction of a rapid vehicle in supercavitating flow, Int. J. Nav. Arch. Ocean 9 (2017) 35–44.

[5] J.P. Rothstein, Slip on superhydrophobic surfaces, Annu. Rev. Fluid Mech. 42 (2010) 89–109.

[6] G. McHale, M.I. Newton, N.J. Shirtcliffe, Immersed superhydrophobic surfaces: gas exchange, slip and drag reduction properties, Soft Matter 6 (2010) 714–719.

[7] E. Aljallis, M.A. Sarshar, R. Datla, V. Sikka, A. Jones, C.-H. Choi, Experimental study of skin friction drag reduction on superhydrophobic flat plates in high Reynolds number boundary layer flow, Phys. Fluids 25 (2013) 025103.

[8] J. Gose, K. Golovin, M. Boban, J. Mabry, A. Tuteja, M. Perlin, S. Ceccio, Characterization of superhydrophobic surfaces for drag reduction in turbulent flow, J. Fluid Mech. 845 (2018) 560–580.

[9] C. Lee, C.H. Choi, C.J. Kim, Superhydrophobic drag reduction in laminar flows: a critical review, Exp. Fluids 57 (2016) 176.

[10] H. Park, C.H. Choi, C.J. Kim, Superhydrophobic drag reduction in turbulent flows: a critical review, Exp. Fluids 62 (2021) 229.

[11] M. Liravi, H. Pakzad, A. Moosavi, A. Nouri-Borujerdi, A comprehensive review on recent advances in superhydrophobic surfaces and their applications for drag reduction, Prog. Org. Coat. 140 (2020) 105537.

[12] X. Feng, P. Sun, G. Tian, Recent developments of superhydrophobic surfaces (SHS) for underwater drag reduction Opportunities and challenges, Adv. Mater. Interfaces 9 (2021) 2101616.

[13] B.R. Gruncell, N.D. Sandham, G. McHale, Simulations of laminar flow past a superhydrophobic sphere with drag reduction and separation delay, Phys. Fluids 25 (2013) 043601.

[14] A. Busse, N.D. Sandham, G. McHale, M.I. Newton, Change in drag, apparent slip and optimum air layer thickness for laminar flow over an idealised superhydrophobic surface, J. Fluid Mech. 727 (2013) 488–508.

[15] T. Jung, H. Choi, J. Kim, Effects of the air layer of an idealized superhydrophobic surface on the slip length and skin-friction drag, J. Fluid Mech. 790 (2016) R1.

[16] J.D. Berry, I.U. Vakarelski, D.Y.C. Chan, S.T. Thoroddsen, Navier slip model of drag reduction by Leidenfrost vapor layers, Phys. Fluids 29 (2017) 107104.

[17] J. Arrieta, A. Sevilla, On the flow separation mechanism in the inverse Leidenfrost regime, J. Fluid Mech. 897 (2020) A4.

[18] W.S. Bradfield, R.O. Barkdoll, J.T. Byrne, Some effects of boiling on hydrodynamic drag, Int. J. Heat. Mass Transf. 5 (1962) 615–622.

[19] Y. Zvirin, G.R. Hewitt, D.B.R. Kenning, Boiling on free-falling spheres: drag and heat transfer coefficients, Exp. Heat. Transf. 3 (1990) 185–214.

[20] I.U. Vakarelski, J.O. Marston, D.Y.C. Chan, S.T. Thoroddsen, Drag reduction by Leidenfrost vapor layers, Phys. Rev. Lett. 106 (2011) 214501.

[21] I.U. Vakarelski, D.Y.C. Chan, S.T. Thoroddsen, Leidenfrost vapour layer moderation of the drag crisis and trajectories of superhydrophobic and hydrophilic spheres falling in water, Soft Matter 10 (2014), 5662-5568.

[22] I.U. Vakarelski, J.D. Berry, D.Y.C. Chan, S.T. Thoroddsen, Leidenfrost vapor layers reduce drag without the crisis in high viscosity liquids, Phys. Rev. Lett. 117 (2016) 114503.

[23] A. Jetly, I.U. Vakarelski, Z. Yang, S.T. Thoroddsen, Giant drag reduction on Leidenfrost spheres evaluated from extended free-fall trajectories, Exp. Therm. Fluid Sci. 102 (2019) 181–188.

[24] D. Saranadhi, D. Chen, J.A. Kleingartner, S. Srinivasan, R.E. Cohen, G.H. McKinley, Sustained drag reduction in a turbulent flow using a low-temperature Leidenfrost surface, Sci. Adv. 2 (2016) e1600686.

[25] E. Achenbach, Experiments on the flow past spheres at very high Reynolds numbers, J. Fluid Mech. 54 (1972) 565–575.

[26] G. McHale, N.J. Shirtcliffe, C.R. Evans, M.I. Newton, Terminal velocity and drag reduction measurements on superhydrophobic spheres, Appl. Phys. Lett. 94 (2009) 064104.

[27] A. Jetly, I.U. Vakarelski, S.T. Thoroddsen, Drag crisis moderation by thin air layers sustained on superhydrophobic spheres falling in water, Soft Matter 14 (2018) 1608–1613.

[28] M.M. Mansoor, I.U. Vakarelski, J.O. Marston, T.T. Truscott, S.T. Thoroddsen, Stable–streamlined and helical cavities following the impact of Leidenfrost spheres, J. Fluid Mech. 823 (2017) 716–754.

[29] I.U. Vakarelski, E. Klasboer, A. Jetly, M.M. Mansoor, A.A. Aguirre-Pablo, D.Y. C. Chan, S.T. Thoroddsen, Self-determined shapes and velocities of giant near-zero drag gas cavities, Sci. Adv. 3 (2017) e1701558.

[30] I.U. Vakarelski, A. Jetly, S.T. Thoroddsen, Stable-streamlined cavities following the impact of non-superhydrophobic spheres on water, Soft Matter 15 (2019) 6278–6287.

[31] I.U. Vakarelski, F. Kamoliddinov, A. Jetly, S.T. Thoroddsen, When superhydrophobicity can be a drag: ventilated cavitation and splashing effects in hydrofoil and speed-boat models tests, Colloids Surf. A 628 (2021) 127344.

[32] F. Kamoliddinov, I.U. Vakarelski, S.T. Thoroddsen, Hydrodynamic regimes and drag on horizontally pulled floating spheres, Phys. Fluids 33 (2021) 093308.

[33] F. Kamoliddinov, I.U. Vakarelski, S.T. Thoroddsen, T.T. Truscott, Skipping under water: Buoyant sphere hydrodynamics at the air–water interface, Phys. Fluids 35 (2023) 072106.

[34] I.U. Vakarelski, N.A. Patankar, J.O. Marston, D.Y.C. Chan, S.T. Thoroddsen, Stabilization of Leidenfrost vapour layer by textured superhydrophobic surfaces, Nature 489 (2012) 274–277.

[35] H. Dong, M. Cheng, Y. Zhang, H. Wei, F. Shi, Extraordinary drag-reducing effect of a superhydrophobic coating on a macroscopic model ship at high speed, J. Mater. Chem. A 1 (2013) 5886–5891.

[36] S.S. Zhang, X. Ouyang, J. Li, S. Gao, S. Han, L. Liu, H. Wei, Underwater drag-reducing effect of superhydrophobic submarine model, Langmuir 31 (2015) 587–593.

[37] N. Wang, L. Tang, Y. Cai, W. Tong, D. Xiong, Scalable superhydrophobic coating with controllable wettability and investigations of its drag reduction, Colloids Surf. A 555 (2018) 290–295.